

The Virtual NMR Spectrometer: A Computer Program for Efficient Simulation of NMR Experiments Involving Pulsed Field Gradients

Peter Nicholas,¹ David Fushman,² Vladislav Ruchinsky,³ and David Cowburn

The Rockefeller University, 1230 York Avenue, New York, New York 10021

Received November 12, 1999; revised February 29, 2000

This paper presents a software program, the Virtual NMR Spectrometer, for computer simulation of multichannel, multidimensional NMR experiments on user-defined spin systems. The program is capable of reproducing most features of the modern NMR experiment, including homo- and heteronuclear pulse sequences, phase cycling, pulsed field gradients, and shaped pulses. Two different approaches are implemented to simulate the effect of pulsed field gradients on coherence selection, an explicit calculation of all coherence transfer pathways, and an effective approximate method using integration over multiple positions in the sample. The applications of the Virtual NMR Spectrometer are illustrated using homonuclear COSY and DQF COSY experiments with gradient selection, heteronuclear HSQC, and TROSY. The program uses an intuitive graphical user interface, which resembles the appearance and operation of a real spectrometer. A translator is used to allow the user to design pulse sequences with the same programming language used in the actual experiment on a real spectrometer. The Virtual NMR Spectrometer is designed as a useful tool for developing new NMR experiments and for tuning and adjusting the experimental setup for existing ones prior to running costly NMR experiments, in order to reduce the setup time on a real spectrometer. It will also be a useful aid for learning the general principles of magnetic resonance and contemporary innovations in NMR pulse sequence design. © 2000 Academic Press

Key Words: NMR; pulsed field gradients; computer simulation; Virtual NMR Spectrometer.

INTRODUCTION

Multidimensional NMR spectroscopy is an important tool for characterizing the structure, dynamics, and interactions of biological molecules in solution (1–3). A typical NMR experiment consists of radiofrequency (RF) pulses interspersed with periods of free precession. Although general rules governing

the evolution of the spin density matrix under these conditions are well understood and corresponding analytical tools are available (e.g., (1)), the calculation of spin evolution under the conditions of a real experiment is complex. NMR experiments grow more elaborate and involve longer sequences of radio-frequency pulses and pulsed field gradients (PFGs). It then becomes increasingly difficult to predict the resulting spectra analytically, and efficient simulation methods provide a useful tool for the refinement of these experiments. These difficulties are particularly great for spin systems of high complexity.

A number of computational approaches to the simulation of NMR experiments have been developed. Computer programs implementing the product-operator formalism (e.g., (1)) and computer algebra for analytical derivation of the spin density matrix under certain conditions in an NMR experiment were described in (4, 5). Although helpful in understanding spin evolution in NMR experiments, this approach has limited applicability to multispin systems and to pulse sequences using shaped pulses, extensive phase cycling, or magnetic field gradients. A general approach to numerical simulation of NMR pulse sequences has recently been developed and implemented as an object-oriented toolkit GAMMA (6). While being able to simulate a wide variety of experimental conditions, GAMMA lacks an easy-to-use interface and requires programming expertise to translate a pulse sequence into the program code. SIMPLTN (7) more closely resembles the interface used in spectrometers, but has limited applicability to gradient pulses and shaped RF pulses, and relies heavily on external software for data processing. None of these programs allows simulation of pulse sequences using PFGs. Recently, Jerschow and Muller (8) have presented an efficient method for calculating the attenuating effect of pulsed field gradients on particular coherence transfer pathways. A different approach to simulating PFGs, based on an approximation of integrating the effects of the sequence using multiple positions in the sample, was recently introduced (9).

As simulations grow more complex, the simplicity and accessibility of the software interface become critically important. It is desirable to present the user with an environment that is organized in a familiar way so that extensive effort need not be devoted to acquiring new programming skills. A goal is to

¹ Current address: School of Medicine, University of North Carolina, Chapel Hill, NC 27599.

² To whom correspondence should be addressed. E-mail: fushmad@rockefeller.edu. After August 2000: Center of Biomolecular Structure & Organization, University of Maryland, 1115 Agriculture/Life Science Surge Building, College Park, MD 20742-3360, Fax: 301-314-0386, E-mail: df117@umail.umd.edu.

³ Current address: Department of Computer Science, Yale University, New Haven, CT 06520.

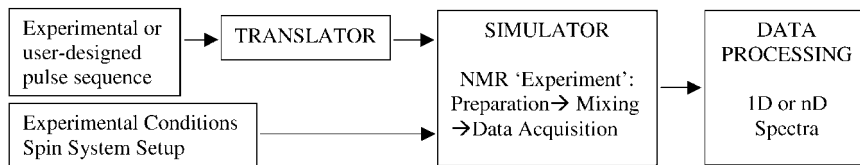


FIG. 1. The flowchart of the Virtual NMR Spectrometer.

permit ease of use by mimicking the operation of NMR spectrometers.

In this paper, we present a software program that addresses these interface issues and uses the most effective features of the previous programs discussed above. This permits the simulation of a wide variety of experiments, including those that employ heteronuclear pulse sequences, phase cycling, pulsed field gradients, and shaped pulses. This software program, the Virtual NMR Spectrometer, simulates multichannel, multidimensional experiments on user-defined spin systems. The program features an intuitive graphical user interface, designed to resemble the appearance and operation of a real spectrometer as closely as possible. This program uses a translator that allows the user to design pulse sequences with the same programming language as in the actual experiment on a real spectrometer. The program incorporates two different approaches to simulate the effect of PFGs on coherence selection: an explicit calculation of all coherence transfer pathways (8) and the approximation method using multiple positions (9). The former is accurate, but slow; the latter requires careful attention to parameterization. In addition, a data processing module is available, which allows all general spectral processing of the calculated free induction decays (e.g., apodization, zero-filling, linear phase correction, and phase-sensitive detection by TPPI, States, States–TPPI, and echo–antiecho methods). For development/debugging of pulse sequences and for learning purposes, the Virtual NMR Spectrometer contains a module that displays the spin density, expressed as a linear combination of basis operators, as it evolves during an experiment.

The Virtual NMR Spectrometer is designed as a useful tool for developing new NMR experiments and for tuning and adjusting the experimental setup for existing experiments, in order to reduce the time on a real spectrometer required for these purposes. It will also be a useful aid in learning general principles of magnetic resonance and contemporary innovations in NMR pulse sequence design.

BASIC FEATURES OF THE VIRTUAL NMR SPECTROMETER

General Outline of the Spectrometer

The principal flowchart of the Virtual NMR Spectrometer is shown in Fig. 1. It features the following basic modules:

(1) *Translator*. A lexical/grammar analysis of the input pulse sequence (using a parser written in Lex (10)) produces a Matlab script *vs_mainsim.m* containing the proper Matlab functions to simulate various steps of spin density evolution and data acquisition according to the algorithms described in the following sections. The current implementation of the translator completely supports the documented features of the Bruker programming language (Versions 2.5 and earlier).

(2) *Simulator*. Given the experimental conditions and user-defined spin system, the simulator executes *vs_mainsim* and produces an “experimental” data set. It currently simulates single- and multichannel 1D and 2D NMR experiments including rectangular and shaped RF pulses and PFGs, performed on a user-defined spin system. Spin-1/2 nuclei (e.g., ^1H , ^{15}N , and ^{13}C) are implemented, and the number of spins is limited only by the size of addressable memory. Other features include spin decoupling and power level selection and switching during experiment, two approaches to simulation of experiments with PFGs (see below), automatic or manual selection of fine steps for calculation of spin density evolution, and tracing and display of various components of the spin density matrix during the time course of the experiment.

(3) *Data processing module*. Processing, visualization, and analysis of the resulting spectrum are implemented. The module allows all typical spectrum processing features, such as apodization, zero-filling, linear phase correction in each dimension, and phase-sensitive detection by TPPI, States, States–TPPI, and echo–antiecho methods. Spectra (real and/or imaginary parts) are displayed as contour plots, which can be zoomed in and/or analyzed as 1D slices in each dimension.

Graphical User Interface

All operation of the Virtual NMR Spectrometer⁴ is performed via a graphical user interface (GUI). This interface is designed to resemble as closely as possible the operation of a real spectrometer, to allow flexibility in selection of various simulation and processing conditions and regimes, and to provide various means of controlling the process of simulation (“experiment”) and its outcome. The main panels and related features/details of the graphical user interface are described below.

⁴ For users familiar with programming, the package allows access and manipulation of various parameters/data from the Matlab shell; after the *vs_mainsim.m* script has been written by the translator, it can be edited using any text editor.

General GUI Panel

This is the main interface panel, which allows the user to activate all other panels, described below. The following actions can be performed directly from this panel: browsing of already existing directories and selection and display of a pulse sequence, starting the translator, selection of the number of spins and of the method of treating PFGs, and starting the simulation of the translated pulse sequence. As the simulation proceeds, the number of t_1 increments already calculated is displayed, as well as the number of counted pathways, in the CTP mode.

Spin Setup Panel

For each nuclear spin, the spin setup panel allows selection of the type of nucleus, its chemical shift position, and spin-relaxation rates, R_1 and R_2 . A built-in program VS_RELMATRIX estimates spin-relaxation rates for each spin or spin transition in a multispin system, given the overall hydrodynamic properties and characteristics of the local mobility of the molecule. A more exact treatment can be optionally provided.

For each pair of spins, the spin setup panel allows selection of the spin-spin coupling and, if necessary, cross-relaxation rates. It toggles the tracing routine to calculate and store the evolution of various components of the spin density operator and allows selection of the basis operators to be traced and displayed.

Pulse Program Parameters

The panel displays all parameters (delays, pulses, power levels, etc.) involved in the pulse sequence, calculates them, if defined via an expression, and allows the user to change their values manually.

Experimental Setup

The experimental setup allows selection of the basic ^1H resonance frequency, channel selection to any other nucleus, channel calibration (user-defined reference power level and the length of the corresponding 90° pulse), selection of carrier frequencies and spectral widths for each channel, number of points in the time domains to be recorded in each experimental dimension, and the number of scans. This panel is also used to set the maximum gradient strength available and the sample length, for the selection of the number of layers, for the AMP approach. A built-in program, VS_SALAMI, automatically updates the list of suggested optimal parameters for simulation of a PFG experiment using the approximate multiposition approach.

Projections Window

The projections window allows tracing/display of the transformation of various components of the spin density matrix and plots projections of the spin density onto user-selected basis

operators as a function of the time/pulse sequence. It also displays the pulse sequence (as a bar diagram with the actual duration of all delays/pulses indicated) on the same time scale as the projection plots. The plot has a zoom-in feature which permits simultaneous expansion of all diagrams along the time axis (horizontally) in order to display fine details.

Data Processing

This panel allows the selection of the following parameters and processing options:

In each dimension, one may select the size of the resulting spectrum, the beginning and end points of the acquired data set to be processed, the shape and the corresponding parameters (width, shift, etc.) of the window function (exponential, Gaussian, trapezoid, sine, qsine) for apodization, and parameters for linear phase correction for processing in the phase-sensitive mode or selection of the magnitude mode.

In the indirectly detected dimension (t_1) the following processing regimes are available for frequency discrimination: TPPI, States, States-TPPI, echo-antiecho.

Processing can be done in each dimension independently, and the real and/or imaginary parts of the resulting interferogram or spectrum can be displayed.

The spectrum display window also allows display of a selected row/column of the resulting spectrum as a 1D plot, and zooming-in on a selected part of the spectrum.

The phase correction window provides a tool for interactive manual phase correction in a selected dimension, F_1 or F_2 .

ALGORITHMS AND METHODS

General Treatment of the Spin Density Matrix under Evolution, Pulses, Delays, and Relaxation

The general product-operator formalism for a quantum mechanical description of the evolution of the spin density matrix under conditions of the NMR experiment is used (1, 3).

All considerations of the spin density evolution are performed in the rotating frame, i.e., in the coordinate frame rotating with the corresponding channel/carrier resonance frequency around the direction of the external magnetic field B_0 (Z axis). In this rotating frame, both the free precession and the effect of a pulse on the spin system can be treated as an evolution under a constant Hamiltonian, with an additional, transverse magnetic field present in the latter case.

Evolution of the Spin Density in the Absence of Pulse Field Gradients

In the absence of magnetic field gradients, it is possible to simulate the effect of a pulse sequence with relatively simple matrix calculations. For a system of coupled spins, the spin

Hamiltonian in the rotating frame can be represented in general form as

$$\begin{aligned} \hat{H} = & - \sum_k [\gamma_k(1 - \delta_k) B_0 - \omega_0] \hat{I}_z^k \\ & + 2\pi \sum_{k,l} (J_{kl}^x \hat{I}_x^k \hat{I}_x^l + J_{kl}^y \hat{I}_y^k \hat{I}_y^l + J_{kl}^z \hat{I}_z^k \hat{I}_z^l) \\ & - \sum_k \gamma_k B_1 (\hat{I}_x^k \cos \phi + \hat{I}_y^k \sin \phi), \end{aligned} \quad [1]$$

where $k, l = 1, \dots, N$ enumerate the spins, γ_k and δ_k are the gyromagnetic ratio and the chemical shielding of the k th spin, J_{kl} is the coupling between spins k and l , B_0 and ω_0 are the constant magnetic field and the carrier frequency for a particular channel, and B_1 and ϕ are the strength and the phase of the applied RF pulse. For example, in the case of a scalar coupling between like spins $J_{kl}^z = J_{kl}^x = J_{kl}^y = J_{kl}$, whereas $J_{kl}^z = J_{kl}$; $J_{kl}^x = J_{kl}^y = 0$ for unlike spins. In a multichannel/heteronuclear experiment, ω_0 , B_1 , and ϕ may differ for different channels. The whole time course of the NMR experiment can be subdivided into consecutive intervals Δt_i characterized by substitutions of experimental variables in the Hamiltonian, Eq. [1]. The transformation of the spin density operator during such an interval, $\Delta t_i = t_{i+1} - t_i$, from an initial state, $\hat{\sigma}(t_i)$, to a final state, $\hat{\sigma}(t_{i+1})$, can be considered the result of the evolution

$$\hat{\sigma}'_{i+1} = e^{-i\hat{H}\Delta t_i} \hat{\sigma}_i e^{i\hat{H}\Delta t_i} \quad [2]$$

and spin relaxation, represented below with the relaxation operator \Re :

$$\hat{\sigma}_{i+1} = \Re \hat{\sigma}'_{i+1} = e^{-R\Delta t_i} (\hat{\sigma}'_{i+1} - \hat{\sigma}_{\text{eq}}) + \hat{\sigma}_{\text{eq}}. \quad [3]$$

Here σ_{eq} is the equilibrium density matrix, and R is the relaxation matrix, including cross-relaxation terms, as necessary. While separating the effects of spin relaxation and evolution is clearly an approximation, the expected errors can be minimized by selecting sufficiently short time intervals Δt_i . Note that the operator $e^{-i\hat{H}\Delta t_i}$ in the right-hand side of Eq. [2] is directly computed as a matrix exponential, without simplifying assumptions.

The effects of spin relaxation are included in a phenomenological fashion, as described by the general relaxation matrix R , consisting of two parts, R_1 and R_2 , corresponding to the longitudinal and transverse relaxation, respectively. Elements of the nondiagonal matrix R_2 describe relaxation rates of various spin transitions, whereas elements of the diagonal matrix R_1 correspond to relaxation of the longitudinal polarization terms. In the current version of the program, the effects of transverse and longitudinal relaxation are treated separately; see, e.g., equations in (11). For the transverse relaxation, the nondiagonal elements of the corresponding spin density matrix

in the right-hand side of Eq. [3] are multiplied elementwise by a matrix composed of the exponential function of the elements of $(-R_2\Delta t_i)$. The effects of cross-relaxation in each pair of spins are treated explicitly, by including the corresponding nondiagonal terms in the R_1 matrix. To account for this effect $\exp(-R_2\Delta t_i)$ is considered a matrix exponential in Eq. [3]. Relaxation of the two-spin order terms in $\hat{\sigma}'_{i+1} - \hat{\sigma}_{\text{eq}}$ is treated separately from the longitudinal polarization of each spin. The program allows the user to define relaxation rates for each nuclear spin or spin transition in a multispin system. These can be calculated using the previously described program DYNAMICS, given the local geometry and interactions (dipolar, CSA) and motional models, including the overall rotational characteristics of the molecule and various models of local mobility (12). The corresponding module, VS_RELMATRIX, is included in the Virtual NMR Spectrometer.

Simulating an NMR experiment therefore requires only the calculation of Hamiltonian matrices (Eq. [1]) for each time interval, to represent the effects of free precession and any RF pulses that will be applied, and the repeated application of Eqs. [2] and [3]. This method of simulating NMR experiments is attractive because of its speed, generality, and simplicity. In the current implementation, no explicit consideration is made of spin equivalence characteristics in the input.

Simulating NMR Experiments with PFGs

Simulating experiments with PFGs requires a more detailed calculation that traces the evolution and mixing of coherences, since the phase acquired by each component of the spin density during a gradient pulse depends on the coherence order, on the gyromagnetic ratios, and on the spatial location of the nuclei involved. It is possible to reconstruct the spin density operator based upon the coherence transfer pathways (CTPs) that contribute to each of the basis operators. The attenuation of each CTP by any gradients in a pulse sequence can be calculated, and the spin density operator will reflect this attenuation. The Virtual NMR Spectrometer provides two methods to account for the effect of PFGs: the calculation of all possible CTPs and the approximate multiposition approach (AMP), which treats the sample as a set of layers (slices).

Calculation of All Possible Coherence Transfer Pathways

Consider, for simplicity, the case of gradients along the axis (Z) of the applied magnetic field, $G_z(t)$, so that the "constant" magnetic field B_0 in Eq. [1] becomes linearly dependent on z : $B_0 \rightarrow B_0 + G_z(t)z$. The time dependence of $G_z(t)$ represents the shape of the PFG. We will also assume that the sample of length L is oriented along the Z axis. The generalization of these results for the general case of a three-axis gradient is straightforward. In the treatment below we follow the approach of counting CTPs suggested in (8).

Attenuation of Coherence Transfer Pathways

During the i th period of free precession, the coherence described by the operator \hat{B}_α acquires a location-dependent phase due to applied gradients,

$$\phi(z)_{\alpha_i} = \gamma_\alpha^* h_i z, \quad [4]$$

where γ^* is the effective gyromagnetic ratio of the coherence (see the Appendix) and

$$h_i = \int_{t_{i-1}}^{t_i} G_z(t) dt. \quad [5]$$

Thus during an experiment with n periods of free precession the m th CTP will acquire a total location-dependent phase

$$\Phi(z)_m = \sum_{i=1}^n \phi(z)_{\alpha_i} = k_m z, \quad [6]$$

where we have introduced the spatial frequency of the m th pathway, k_m .

Location-Dependent Spin Density Operator

Given vector lists $\mathbf{w}_n^{(\alpha)}$ and $\mathbf{k}_n^{(\alpha)}$ that contain the weight and spatial frequency of the CTPs leading to basis operators \hat{B}_α , one can express the location-dependent spin density operator after the application of n RF pulses and/or delay periods as

$$\hat{\sigma}(z) = \sum_{\alpha=1}^{(4^N-1)} [\hat{B}_\alpha \sum_j (w_n^{(\alpha)})_j e^{-i(k_n^{(\alpha)})_j z}], \quad [7]$$

Here the first sum extends over the complete set of basis operators and the second sum extends over all pathways that contribute to the basis operator \hat{B}_α ; $(w_n^{(\alpha)})_j$ and $(k_n^{(\alpha)})_j$ are the complex weight and spatial frequency (respectively) of the j th pathway contributing to the coherent state \hat{B}_α , after the n th evolution period. Note that at present, we neglect molecular translational diffusion in the direction of the gradient. The observable quantity, the spatial average of the density operator, is obtained by integrating Eq. [7] over the sample length, from $z = -L/2$ to $L/2$,

$$\bar{\hat{\sigma}}(z) = \sum_{\alpha}^{4^N-1} [\hat{B}_\alpha \sum_j (w_n^{(\alpha)})_j \text{sinc}((k_n^{(\alpha)})_j L/2)], \quad [8]$$

where L is the sample length. In fact, because the sinc function oscillates and crosses zero, it would be possible to obtain estimates of large attenuation that were extremely sensitive to

gradient size and duration. Therefore the envelope of the sinc function is used to estimate the attenuation by the gradients

$$\text{sinc}_{\text{Env}} = \begin{cases} \frac{\sin(x)}{x}, & 0 \leq |x| \leq \frac{\pi}{2} \\ \frac{1}{|x|}, & \frac{\pi}{2} \leq |x| \end{cases}. \quad [9]$$

Simulating an experiment therefore requires an efficient method of generating the lists $\mathbf{w}_n^{(\alpha)}$ and $\mathbf{k}_n^{(\alpha)}$. These calculations are performed using the transformation matrix, as described in the Appendix, Eqs. [A10]–[A13].

The advantage of this approach is in its simplicity—the evolution of the spin density operator and the transformation matrices are calculated as if the gradients were absent. Once the transformation matrices are derived for each time period Δt_i , the effect of PFGs can be taken into account by counting all possible (or most efficient) coherence transfer pathways, computing the corresponding \mathbf{w} and \mathbf{k} lists, and substituting them into Eq. [8]. The disadvantage is the necessary bookkeeping for a large number of CTPs. In practice, relatively few pathways contribute to the observed signal, relative to the total number of possible pathways for a particular experiment.

Approximate Multiple-Position Approach

A more direct approach to simulating the effect of PFGs is by calculating the exact spin density operator at many locations within the sample, and taking the average of these calculations as the spatial average of the sample magnetization. For example, in the case of a Z -axis gradient, one might slice the sample into N_L layers of equal height, perpendicular to the Z axis (Fig. 2a), and calculate the evolution of the spin density operator in the presence of PFGs for each layer separately (e.g., (9)). The method can be generalized to include triple-axis gradients. For a small number of layers ($N_L \sim 10$ – 20) this method is expected to be more efficient than CTP, in particular, for pulse sequences involving large number of PFGs (hence large number of possible CTPs). However, as outlined in the analysis below, an accurate simulation using this approach might require a much greater number of layers to be considered, e.g., in heteronuclear systems, which could reduce its efficiency compared to the CTP method.

Consider evolution in the presence of a single PFG of the spin density initially placed in the transverse plane. For convenience, we enumerate the layers from $n_z = -a$ to a , so that for an odd number of layers considered here, $N_L = 2a + 1$, and $n_z = 0$ corresponds to the layer located at $z = 0$. The spin density in the $n_z = 0$ layer will be identical to the spin density calculated neglecting gradients. All other layers will acquire a position-dependent phase during the time interval τ ,

$$\phi(n_z) = k_e n_z \frac{L}{N_L}, \quad [10]$$

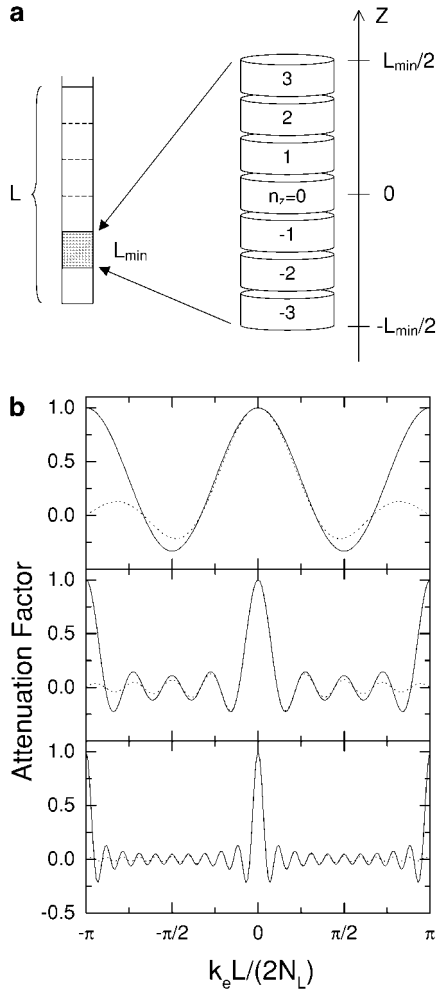


FIG. 2. Illustration of the approximate multiposition approach for the case of the Z-axis gradient: (a) representation of a real sample as a set of “minimal” samples (left) and the layer selection scheme for the representative sample (right); (b) the attenuation factor in Eq. [12] as a function of $k_e L / (2N_L)$ for various N_L . The corresponding sinc function, $\text{sinc}(k_e L / 2)$, is also shown in (b), as dotted lines, for comparison. Only a small, representative interval of $k_e L / (2N_L)$ values is shown here, due to periodicity of the attenuation factor, with a period of π . An increase in the attenuation factor at $k_e L / (2N_L) = \pm\pi$, obvious from (b), is due to zeros of the denominator in Eq. [12], and could lead to simulation artifacts. Rule (3), Eqs. [15] and [17], is designed to keep $k_e L / (2N_L)$ within the $(-\pi/2, \pi/2)$ interval.

where $k_e = \gamma^* h$, $h = \int_0^\tau G(t) dt$, and γ^* is the effective gyromagnetic ratio for a particular component of the spin density (Eq. [A5]). For a more complex experimental scheme, k_e will represent the effective spatial frequency for the entire experiment (see Eqs. [A5] and [A13]):

$$k_e = \sum \gamma_i^* h_i, \quad [11]$$

The spatial average of the spin density component corresponding to a particular value of k_e will be given by

$$\begin{aligned} \overline{\hat{\sigma}_{k_e}} &= \frac{1}{N_L} \sum_{n_z=-a}^a \hat{\sigma}_{k_e}(n_z) = \frac{\hat{\sigma}(0)}{N_L} \sum_{n_z=-a}^a e^{-i\phi(n_z)} \\ &= \hat{\sigma}(0) \left[\frac{1}{N_L} \frac{\sin\left(\frac{k_e L}{2}\right)}{\sin\left(\frac{k_e L}{2N_L}\right)} \right]. \end{aligned} \quad [12]$$

The expression in brackets reflects the attenuation of the signal due to dephasing by PFGs during an experiment. For the desired coherence, i.e., the one to be preserved during the PFG experiment, $k_e = 0$, according to gradient selection rules. As follows from Eq. [12] the desired coherence will be completely preserved by this method, independent of the choice of L and N_L . It is then the undesired coherences, i.e., those to be destroyed by PFGs, which will influence the optimization of the parameters. As anticipated, the attenuation factor in Eq. [12] approaches $\text{sinc}(k_e L / 2)$ as $N_L \rightarrow \infty$. However, because of its periodicity, caused by a finite number of layers, this equation will approximate the sinc function properly only in the interval $|k_e L / (2N_L)| \leq \pi/2$ (Fig. 2b), where the maximum error is approximately equal to $2/N_L$. This might require a large number of layers to be considered for a given sample length L . For example, assuming a typical sample length of 2 cm, one would expect the minimal number of layers for the gradient-selective COSY experiment described below to be ~ 228 . Thus, even for such a simple experiment, one would need to repeat the whole simulation at least 228 times to ensure an accurate result.

Optimization of the Approximate Multiposition Approach: Minimal Sample

A solution to this problem (9) is to perform the simulation for a much smaller representative, or “minimal” sample, of length L_{\min} , thus considering the real sample as a set of many such samples, as illustrated in Fig. 2a. All these representative samples shown in Fig. 2a are virtually identical from the point of view of spin density evolution under PFGs. Consider, for example, a representative sample shifted by jL_{\min} (j is an integer) along the Z axis with respect to the one considered in Eq. [10]. The phase acquired by a spin coherence in a layer n_z in this sample is (see Eq. [13]) $\phi(n_z, j) = k_e(n_z L_{\min} / N_L + jL_{\min}) = \phi(n_z) + 2\pi m j$, which is indistinguishable from $\phi(n_z)$ due to periodicity of the exponential function $e^{-i\phi}$ in Eq. [12]. Note that if the actual sample length L is not a multiple of a particular selected minimal length, L_{\min} , i.e., L/L_{\min} is not an integer, then the error resulting from such an approximation is expected to be of the order or less than $L_{\min}/(2L)$, which still yields a good level of accuracy for large L/L_{\min} .

For a particular undesired coherence with the effective spatial frequency k_e ($k_e \neq 0$), the following criteria apply for the selection of an optimal simulation setup.

(1) The minimal sample length, L_{\min} , can be selected to coincide with one of the zeros of the numerator in Eq. [12], i.e.,

$$L_{\min} = 2\pi m/k_e, \quad [13]$$

where m is any positive integer.

(2) The number of layers must be selected to avoid zeros of the denominator,

$$N_L \neq k_e L / (2\pi n), \quad [14]$$

where n is any positive integer.

(3) To minimize contributions from undesired coherences, the number of layers can be selected to provide the value of the sine function in the denominator in Eq. [12] close to its maximum,

$$N_L \approx k_e L / [\pi(2n + 1)], \quad [15]$$

where $n = 0, 1, \dots$. The optimal number of layers, N_L , is then the nearest integer to the value in the right-hand side of this equation. Rule (3) is rather “the rule of thumb” and does not have to be strictly obeyed, as rule (2).

Combining rules (1) and (2) gives $N_L \neq m/n$; i.e., for a given m , one should avoid situations when N_L is a factor of m . For example, any $N_L > m$ should work. From rules (1) and (3) one obtains $N_L \approx 2m/(2n + 1)$.

While rule (1) helps optimize the sample length, rules (2) and (3) determine the optimal number of slices for the multi-layer simulation, hence the efficiency of the simulation. If rule (2) is not obeyed, the expression in brackets in Eq. [12] equals 1; i.e., the corresponding (undesired) coherence will be completely preserved, which, therefore, might lead to severe calculational error (see Figs. 6b and 6c below). A failure to obey rule (1) will also result in a nonzero contribution from undesired coherence to the resulting calculation. This contribution, however, is usually smaller (Fig. 2b) and could be further reduced by maximizing the denominator in Eq. [12] (see rule (3)) and by selecting a sufficiently large number of layers, although at a cost of increased simulation time. Since for $N_L > 1$ the denominator in Eq. [12] is oscillating slower than the numerator, selecting N_L close to $k_e L / \pi$ (rule (3), $n = 0$) will automatically ensure that rule (2) is obeyed.

When several coherences have to be suppressed simultaneously, the optimization becomes more complex. Consider a set of k_e values: $\{k_{e1}, \dots, k_{en}\}$. For the optimized sample length L_{\min} , application of rule (1) to all these k_e suggests that in order to meet the optimal conditions, all the following ratios have to give integer numbers:

$$\begin{aligned} m_1 &= L_{\min} k_{e1} / (2\pi); & m_2 &= L_{\min} k_{e2} / (2\pi), \dots; \\ m_n &= L_{\min} k_{en} / (2\pi). \end{aligned} \quad [16]$$

This then requires finding the least L_{\min} , which is still large enough so that all the ratios in the right-hand side of these equations can be considered integers, to a good approximation.

According to rule (3), a simple recipe for selection of N_L is then

$$N_L \geq \max\{k_e\} L_{\min} / \pi, \quad [17]$$

where $\max\{k_e\}$ is the largest entry in the $\{k_e\}$ set, usually $\Sigma|\gamma_i^*| \Sigma|h_i|$. This will ensure that all other values of $k_e L / (2N_L)$ are within the $(-\pi/2, \pi/2)$ interval (Fig. 2b), thus obeying rule (2). A program routine VS_SALAMI is included in the program, which performs automatic determination of L_{\min} and a minimal N_L given the pulse sequence and the experimental setup.

Practical Suggestions

To summarize the above considerations, let us perform simple estimations. If $\min\{k_e\}$ denotes the smallest nonzero absolute k_e value, then, at least, the following relation should hold:

$$L_{\min} = 2\pi / \min\{k_e\}. \quad [18]$$

Combined with Eq. [18] this leads to the following estimate for the number of layers necessary for an accurate simulation of the PFG experiment using the AMP approach:

$$N_L \geq 2 \max\{k_e\} / \min\{k_e\}. \quad [19]$$

These values of simulation parameters, L_{\min} and N_L , will then ensure that the whole range of possible undesired coherence pathways is reasonably well suppressed. As follows from Eq. [19], the number of layers, which determines the computational efficiency of the AMP approach, could become large, in particular, in experiments involving nuclei with significantly different gyromagnetic ratios (e.g., $N_L > 2\gamma_H / |\gamma_N| \sim 20$ for experiments with ^{15}N and ^1H), and/or many-spin systems with large possible coherence orders.

It is worth noting here that the optimal parameters for the AMP approach depend on the gradient strength. If a single gradient pulse is applied during the pulse sequence, then $k_e \propto G$, and therefore L_{\min} is inversely proportional to the gradient strength. The optimal number of layers, N_L , however, does not depend on the strength of the applied gradient (cf. Eq. [19]). In the case of multiple PFGs present in the pulse sequence, the situation is less straightforward, since the spatial frequency, k_e , is a linear combination of various gradients present in the pulse sequence (Eqs. [11], [A5], [A13]). However, considerations similar to those for a single gradient could be applied to the

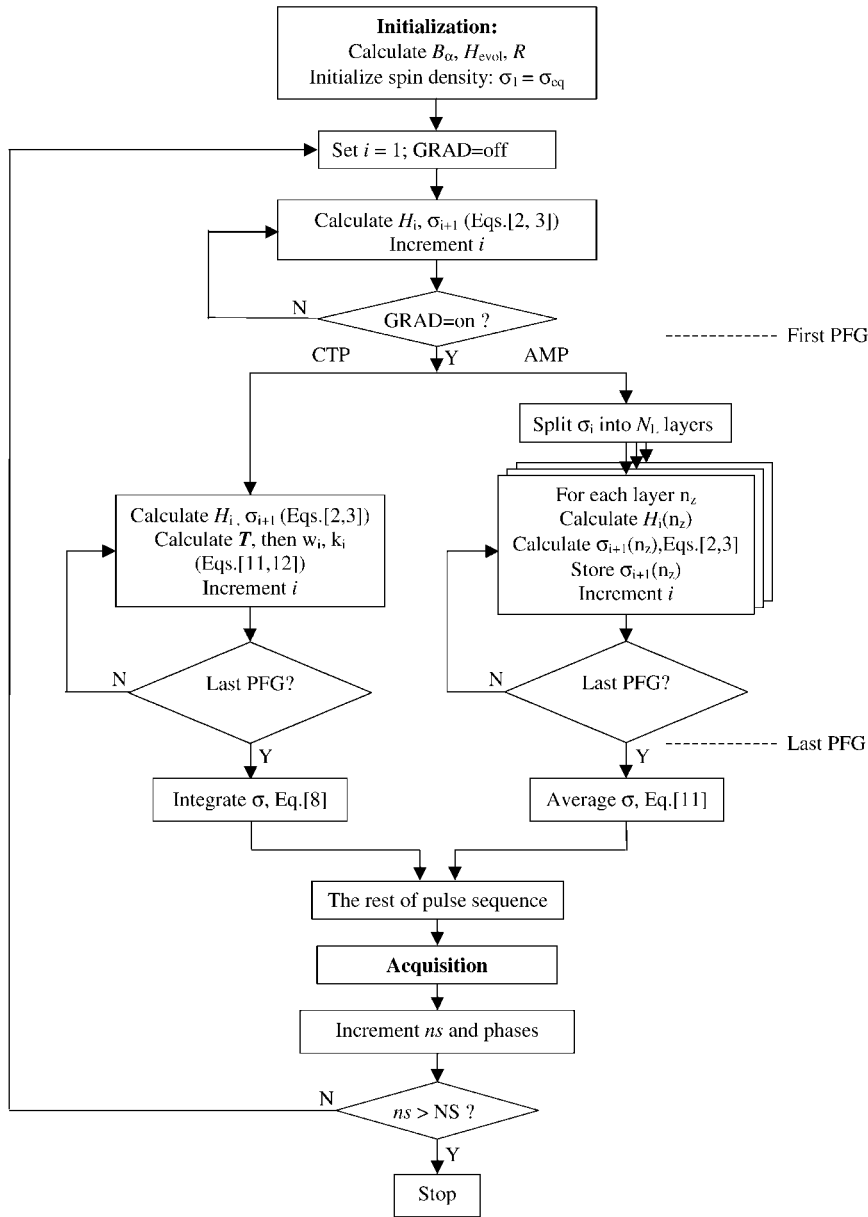


FIG. 3. Flowchart of the experiment simulation module for an NMR experiment with PFGs. The two available modes, CTP and AMP, for simulation of a gradient experiment are illustrated. For simplicity, a one-dimensional experiment is shown. The flowchart for a simulation of an experiment without PFGs is not shown; however, this simulation can be considered the approximate multiposition approach scheme with $N_L = 1$ and $n_z = 0$.

dependence of the optimal parameters on the overall level of the gradient strength, i.e., when all gradients are scaled uniformly.

Simulation Algorithm

Here we describe how the NMR experiment is simulated in the Virtual NMR Spectrometer.

As the result of translation of a pulse program (see description of the translator), the whole duration of the sequence is divided into N intervals of constant Hamiltonian; i.e., during

each interval the applied magnetic fields B_1 and their phases on all channels are constant (or zero). In those cases when a (slow) modulation of H takes place (e.g., shaped RF pulses or shaped PFGs in the approximate multiposition approach), the length of the time interval Δt_i is chosen not to exceed the step size in the numerical approximation of the corresponding shape function. In addition, the evolution periods can be subdivided in smaller intervals, selected automatically ($\Delta t_i < 1/(\pi \max[J_{ki}])$) or user defined, to represent more accurately the effect of relaxation and/or precession under spin couplings.

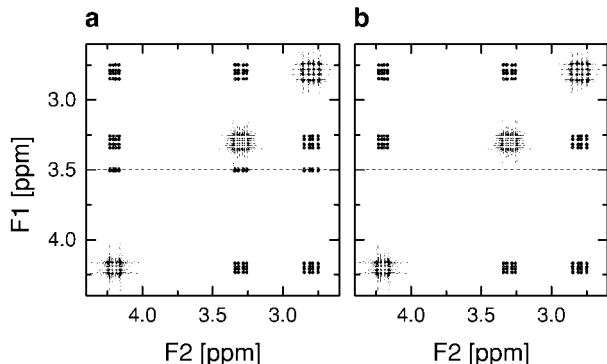


FIG. 4. An example of the simulated COSY experiment for a three-proton system. The spectra were obtained (a) with only one scan and (b) with the full phase cycle. Axial noise present in (a) is suppressed in (b) by the phase cycling. The carrier position in F_1 is indicated by a dashed line. The pulse program used for the simulation was *cosysh* from the standard Bruker pulse program library. The proton chemical shift positions and scalar couplings were as follows: $H^\alpha = 4.2$ ppm, $H^\beta = 2.8$ ppm, $H^\gamma = 3.3$ ppm, $J_{\alpha\beta} = 20$ Hz, $J_{\alpha\gamma} = 12$ Hz, $J_{\beta\gamma} = 30$ Hz. This spin system mimics nonlabile protons in cysteine; the couplings were assumed to be greater than the actual ones for illustrative purposes. The spectrometer frequency was set to 500 MHz. Spectra were acquired with 256 t_1 increments, each containing 128 complex points in t_2 . The simulated “experimental” data were zero-filled up to 256×256 complex points and processed using the States method. The 90° shifted sine-bell function was used for apodization.

The execution of a translated pulse sequence in an experiment involving PFGs includes the following main steps, indicated on the flowchart in Fig. 3.

Initialization

Given the spin system, the program calculates all basis operators, \hat{B}_α , the basic Hamiltonian, \hat{H}_{evol} , for the free evolution, and, if in the CTP mode, h_i . The spin density matrix is set to initial value, determined by the equilibrium state (e.g., $\sigma_{\text{eq}} = \sum \gamma_k I_{kz}$ or based on user-defined populations of spin levels or various spin systems). If CTP mode, set all $w_0^{(\alpha)} = []$ and $\mathbf{k}_0^{(\alpha)} = 0$.

Simulation of the Pulse Sequence

For each time period (free precession or pulse), spin density evolution is calculated according to Eqs. [2] and [3]. If RF pulses are present, the corresponding terms are added to the Hamiltonian. If the pulse sequence contains no gradient pulses, these steps will be repeated until the end of the pulse sequence is reached.

Prior to the first gradient pulse, the corresponding user-selected gradient-simulation mode, CTP or approximate multiposition, is activated. In the CTP mode, the transformation matrix is calculated and the pathway lists are generated, according to Eqs. [A10]–[A13]. These calculations are repeated along with the simulation of the spin density evolution until the end of the last gradient in the pulse sequence. After that, the

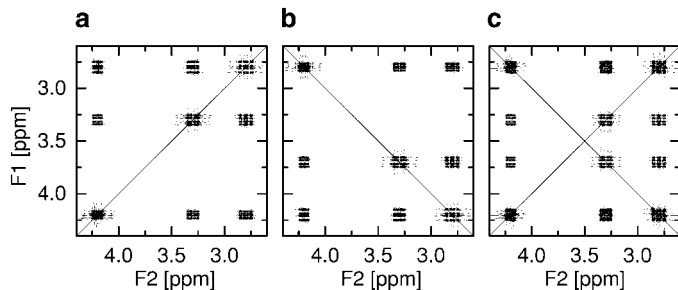


FIG. 5. Simulated homonuclear COSY experiment using gradient selection (gs-COSY (14)). The pulse program used for this experiment was *cosygs* (Bruker). Shown are spectra corresponding to gradient selection of (a) P -type coherence (p peaks), (b) N -type coherence (n peaks), and (c) no coherence selection, when both p and n peaks are present. Spectra shown in this figure were obtained using the coherence transfer pathways approach. The sample length was set to 2 cm. Positions of the diagonal peaks are indicated by the corresponding diagonal lines. All spectra were acquired with 256 t_1 increments containing 128 complex points in t_2 . The simulated data were zero-filled up to 256×256 points and apodized using a 90° shifted sine-bell function. Processing was done in the magnitude mode. The gradient pulses (1 ms duration) were sine-shaped, 1 ms long, with a maximum gradient strength of 21 G/cm and gradient ratios of 1:1 for the p peaks and 1:–1 for the n peaks. The spin system was the same as that in Fig. 4.

“integrated” spin density is calculated according to Eq. [8], and the simulation proceeds in the normal (nongradient) mode. As the number of possible CTPs increases dramatically with the number of pulses, a threshold value can be set for the weights w_j , so that only those pathways which have significant weight will be included in the generated pathway lists.

During each period of evolution, mixing of coherences will occur with different strengths. Some mixing will be strong (of

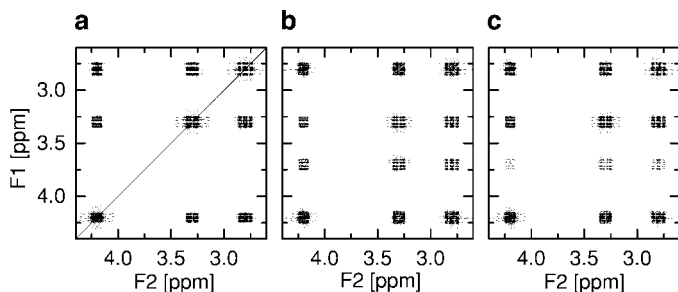


FIG. 6. Same gs-COSY experiment as in Fig. 5a, simulated using the approximate multiposition approach. The optimal simulation parameters for suppression of all undesired coherences were estimated according to Eqs. [18] and [19] as $N_L = 12$ and $L_{\text{min}} = 0.0176$ cm ($\min\{k_e\} = 358$ rad/cm). The spectrum shown in panel (a) was calculated using the simulation conditions close to optimal: $N_L = 13$ and $L_{\text{min}} = 0.0176$ cm. Panels (b) and (c) illustrate artifacts caused by deviations of one of these parameters from the optimal values: $N_L = 5$ in (b) while $L = 6L_{\text{min}}$ in (c). These deviations are selected to provide simulation parameters close to violation of rule (2) (Eq. [14]) for suppression of the n peaks. The additional signals and spectral distortions present in (b) and (c) are artifacts due to incomplete suppression of the undesired coherences, caused by deviation of the simulation parameters from their optimal values. The spin system, pulse program, and all other experimental and processing conditions are the same as those in Fig. 5.

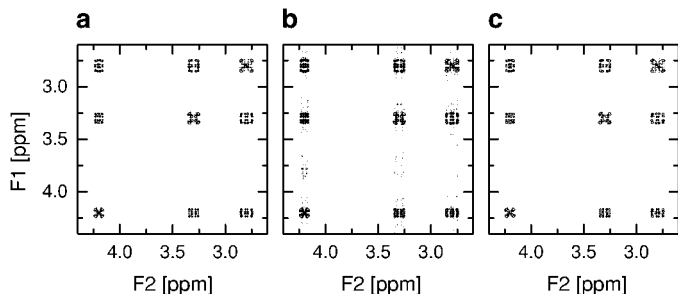


FIG. 7. An example of a double-quantum-filtered COSY using gradient selection (gs-DQF-COSY (14)). The pulse program was *cosygpmpfp* (Bruker). The spectra in (a) and (b) were simulated using the coherence transfer pathways approach, with the number of pathways retained per basis operator set to 10 and 4, respectively. The spectrum in (c) was calculated using the approximate multiposition approach with $L_{\min} = 0.035$ cm and $N_L = 19$. Spectral artifacts in (b) are due to reduction in the number of accounted pathways. The spin system and the size of acquired data are the same as those in Fig. 4. The 1-ms gradient pulses were sine-shaped, with maximal strengths of 10.5 and 21 G/cm (for the double-quantum coherence selection). The “experimental” data were zero-filled and apodized using a 90° -shifted squared sine bell. Processing was performed using TPPI. A 90° zero-order phase correction was applied in both dimensions (14).

order 1) and will ultimately generate the predominant signal observed in an experiment. There will also be weaker (of order 10^{-3}) mixing, due, for example, to pulse imperfections, and these will generally be more numerous than the strong mixing. In the absence of cross-relaxation, the mixing between two states must always be less than or equal to unity. (In the case of cross-relaxation rates corresponding to those physically observed, this statement remains approximately true.) Therefore if one knows the weight of a particular pathway at a certain point in an experiment, one can be certain that all the progeny of that pathway (i.e., the CTPs that result from branching of the pathway with known weight as further evolution and mixing occur) will have equal or lesser weight than the original pathway did. It follows that if one is willing to accept a small reduction in accuracy in exchange for an increase in speed, one can set a threshold value and after each and every period of evolution retain only those “significant” pathways that have weight greater than the threshold. When such an approach is adopted, the number of pathways and therefore the calculation time for a given simulation can be greatly reduced.

An alternative method offers an advantage over the one just described because it simplifies the process of determining an appropriate threshold value. Instead of setting a threshold that the pathway weights must exceed for a CTP to be counted, one can sort the list of pathways according to weight after each period of evolution, and retain only the n_p most significant pathways. In practice, for the experiments presented here, we found that setting n_p to 10–20 CTPs per basis operator \hat{B}_α provides a reasonable compromise. Reducing n_p below 10 does not increase speed significantly and eventually generates incorrect spectra; cf. Fig. 7b below. This method appears to be generally applicable to all experiments, and does not appear to

reduce the efficiency of the suppression of unwanted coherences.

In the approximate multiposition mode, the calculation is split into separate calculations of spin density evolution for each layer. A set of N_L matrices $\sigma_i(n_z)$ is generated by duplicating the spin density matrix, σ_i , prior to the occurrence of the first gradient. For each time interval, the calculation of spin density evolution, Eqs. [2] and [3], is then performed N_L times, with the longitudinal magnetic field $B'_0 = B_0 + Gn_z L_{\min}/N_L$ in the Hamiltonian (Eq. [1]). The resulting spin density matrix, $\sigma_{i+1}(n_z)$, is stored for each layer. After the last gradient pulse, the spin density matrix is averaged over all spin densities calculated separately for each layer.

Acquisition

Based upon $\bar{\sigma}$, the FID is acquired and stored.

The acquisition period is divided into $td2$ equal evolution

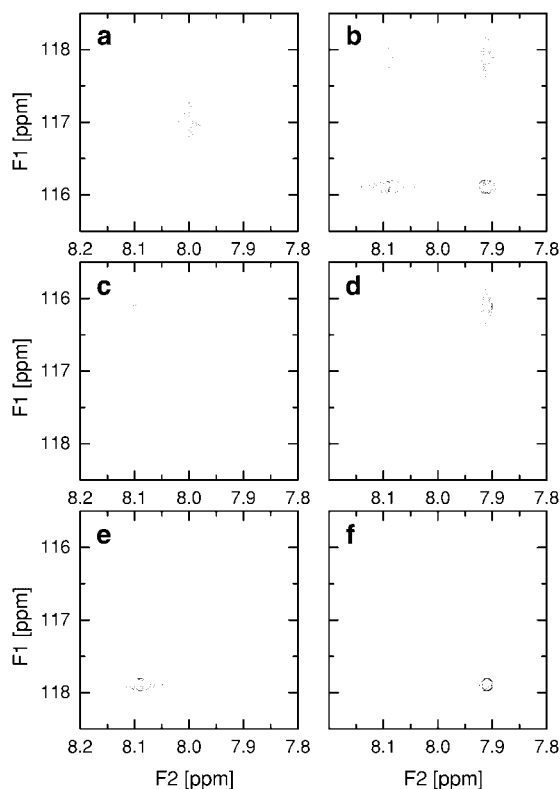


FIG. 8. Illustration of $^1\text{H}\{^{15}\text{N}\}$ HSQC/TROSY experiments. (a) Decoupled $^1\text{H}\{^{15}\text{N}\}$ HSQC spectrum; (b) coupled $^1\text{H}\{^{15}\text{N}\}$ HSQC spectrum resolving all four NMR signals of the $^1\text{H}\text{--}^{15}\text{N}$ spin pair; (c)–(f) generalized TROSY-type experiments selecting one of the four cross peaks at a time (according to (15)). The pulse sequences used were (a, b) *invtp* from the standard Bruker library and (c–f) α/β -HSQC- α/β described in (15). The chemical shift positions were assumed to be at 8 ppm (^1H) and 117 ppm (^{15}N), and the scalar coupling was set to 90 Hz. Processing was performed using TPPI (a and b) or as described in (15) (c–f). The relaxation rates for the individual transitions were calculated using the VS_RELMATRIX module, assuming an overall rotational correlation time of 10 ns and a spectrometer frequency of 500 MHz.

intervals of length determined by the desired spectral width in F_2 ; the spin density evolution is calculated using the same approach (Eqs. [2] and [3]) as during the pulse sequence. Spin decoupling is applied to a selected channel as necessary. Prior to each evolution interval, quadrature detection of the signal (FID) is performed by calculating transverse magnetization components for the directly detected nuclear channel.

This sequence of events is repeated according to the number of scans and to the number of t_1 increments in a 2D experiment, determined by the user.

The Virtual NMR Spectrometer is written in Matlab (MathWorks). This language provides an easy and intuitive tool for various manipulations involving matrices and cell arrays of any dimension. Matlab is currently available on practically any platform. The program can be run from the Matlab shell or, alternatively, can be exported as C/C++ code, and compiled and run as a stand-alone application.

RESULTS AND DISCUSSION

Examples of Spectra Simulations Using the Virtual NMR Spectrometer

Here we consider some typical examples to illustrate the ability of the Virtual NMR Spectrometer to simulate NMR experiments.

Figure 4 depicts a region of the 2D COSY spectrum simulated using a standard pulse sequence without PFGs, and also illustrates suppression of axial peaks by a full phase cycle. The spin system parameters, experimental setup, and data processing parameters are listed in the legend to the figure. The same spectrum, obtained using a pulse sequence with gradient selection (gs-COSY), is shown in Figs. 5 and 6. Figure 5 also illustrates the ability to select the desired coherence by changing the relative sign of the gradients. These spectra were calculated using the CTP approach. The multilayer approach yielded identical spectra, as shown in Fig. 6a. Figures 6b and 6c also illustrate the sensitivity of this method to proper optimization of the simulation parameters, L_{\min} and N_L .

Simulation of a homonuclear double-quantum COSY experiment using gradient selection yielded 2D spectra shown in Fig. 7. The spectra obtained using CTP and AMP methods under optimal conditions are virtually identical. Figure 7b also illustrates the limitation of the truncated CTP method with respect to the minimal number of pathways retained per basis operator.

Heteronuclear ^1H - ^{15}N correlation experiments are illustrated in Fig. 8. We simulated a standard HSQC experiment, with a 180° ^1H decoupling pulse present during ^{15}N evolution and ^{15}N decoupling during acquisition (Fig. 8a) and the coupled four-peak spectrum is shown in Fig. 8b. Differences in the line-widths/intensities of various cross peaks are due to differences in the transverse relaxation rates for the corresponding single-quantum coherences. TROSY techniques (I_3) have been re-

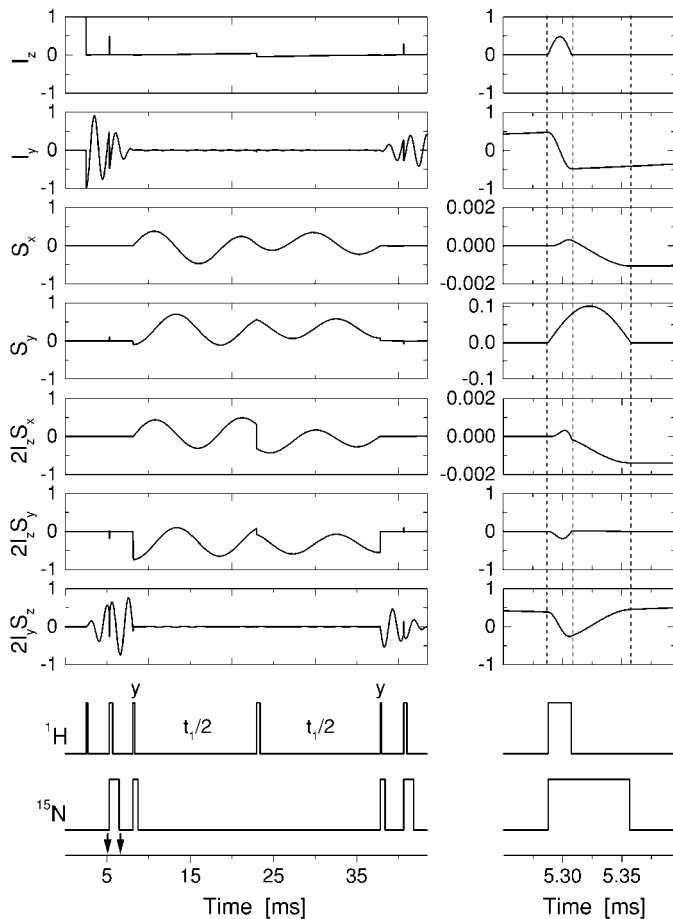


FIG. 9. The evolution of individual components of the spin density operator calculated during a pulse sequence. Left-hand panels depict the time evolution of selected spin density components (labeled at left) during one scan in a t_1 transient for the $^1\text{H}\{^{15}\text{N}\}$ HSQC experiment. Panels on the right show an expansion of these plots (indicated by arrows in the pulse sequence on the left panel), to illustrate details of the spin density evolution from 180° pulses applied on both ^1H and ^{15}N channels, during INEPT transfer from ^1H to ^{15}N . I and S denote ^1H and ^{15}N spin operators, respectively. The corresponding pulse sequence is shown at the bottom. Thin and thick bars (left panel) indicate schematically 90° and 180° pulses, respectively; the pulses are along the x axis, unless indicated. The pulse diagram on the right panel represents the actual duration of the pulses. The pulse sequence, the experimental conditions, and the spin system are same as those in Fig. 8a, except that the carriers on both channels were offset here by 1 ppm, to illustrate the evolution under chemical shifts. Fine sampling of spin density evolution was achieved by dividing each interval of the constant Hamiltonian into 40 small time steps. The equilibrium spin density was set to $I_z + (\gamma_{\text{N}}/\gamma_{\text{H}})S_z$. The right panels illustrate features arising from the finite duration of the pulses. The hump seen in the I_z plot during the ^1H 180° pulse (right panel) reflects the temporary longitudinal component of ^1H magnetization appearing when transverse magnetization (y component) is being rotated by 180° around the x axis, from the $+y$ to $-y$ direction. Similarly, the temporary S_y magnetization is associated with the rotation of the longitudinal ^{15}N magnetization (S_z) around the x axis, from the $-z$ to $+z$ direction, caused by the 180° ^{15}N pulse. The evolution of this transient S_y component under the chemical shift and the J coupling, in turn, leads to small S_x and $2I_zS_x$ components, respectively, seen on the corresponding panels on the right.

cently suggested, which take advantage of the low transverse relaxation rate for the coherence corresponding to the lower-right cross peak in Fig. 8b. Figures 8c–8f illustrate the ability of the program to simulate these experimental approaches, designed to select only one particular cross peak and suppress all other, undesired peaks.

As noted above, the Virtual NMR Spectrometer permits one to track and display the evolution of individual components of the spin density during the time course of the experiment. This is illustrated in Fig. 9 for the HSQC experiment. Explicit calculation of all events, including pulses, in the pulse sequence reveals fine details of the evolution of spin density components, using sufficiently small time increments.

CONCLUSIONS

The Virtual NMR Spectrometer demonstrated here allows computer simulation of NMR experiments, including most features of modern experimental design. A combination of computational efficiency with considerable flexibility and ease of use makes it a powerful tool for pulse sequence design and for testing and tuning preexisting sequences and experimental conditions, prior to running costly NMR experiments. The Virtual NMR Spectrometer can also be used for learning the general principles of magnetic resonance spectroscopy and for training in pulse sequence design and data processing. The source code, manual, and demo examples for the Virtual NMR Spectrometer are planned to be available for ftp download from the Web page www.v-mr.org/vnmr.

APPENDIX

Basis Spin Operators

The basis formed by the Cartesian spin operators \hat{I}^x , \hat{I}^y , \hat{I}^z , the product operators, and the identity operator, E , provides an intuitive understanding of NMR experiments in terms of rotations of vectors. An alternative basis, formed by replacing the \hat{I}^x and \hat{I}^y operators with the shift (raising and lowering) operators \hat{I}^+ and \hat{I}^- is much more useful for describing an experiment in terms of coherence transfer pathways since \hat{I}^+ and \hat{I}^- have coherence order $p = +1$ and $p = -1$, respectively, whereas \hat{I}^x and \hat{I}^y both represent mixtures of coherence orders $+1$ and -1 . This spherical basis set (3) is used here to calculate the dephasing effects of PFGs during an experiment in the CTP mode. In order to explicitly define the basis, we first define the spin operators

$$\hat{I}_q^r = \begin{cases} \hat{E}, & r = 0 \\ \hat{I}_q^-, & r = 1 \\ \hat{I}_q^z, & r = 2 \\ \hat{I}_q^+, & r = 3 \end{cases} \quad [\text{A1}]$$

where q is an index over all nuclear spins.

We also define the operation $\mathbf{b}_4[n]$ that creates from a base 10 natural number, n , a vector whose components are a base 4 representation of n such that if $\delta_4 = \mathbf{b}_4[d]$, then $\sum_i \delta_i (4^{i-1}) = d$. So, for example, $\mathbf{b}_4[7] = \langle 3, 1 \rangle$. Note that in the notation used here the indices, δ_i , corresponding to increasing powers of 4 are ordered from left to right. Then the complete set of $4^N - 1$ nontrivial basis operators, the \hat{B}_α , can be calculated from (1)

$$\hat{B}_\alpha = 2^{\eta-1} \prod_{q=1}^N I_q^{b_q}, \quad [\text{A2}]$$

where $\mathbf{b} = \mathbf{b}_4[\alpha]$, $\mathbf{b}_4[\alpha]$ is understood to have N elements (leading zeros if necessary), and η is equal to the number of nonzero elements in $\mathbf{b}_4[\alpha]$. For example, $\mathbf{b}_4[17] = \langle 1, 0, 1 \rangle$ corresponds to $\eta = 2$ and $\hat{B}_\alpha = 2\hat{I}_1^z\hat{I}_3^-$; $\mathbf{b}_4[21] = \langle 1, 1, 1 \rangle$ corresponds to $\eta = 3$ and $\hat{B}_\alpha = 4\hat{I}_1^-\hat{I}_2^-\hat{I}_3^-$. In a two-spin system, for example, the \hat{B}_α would be

$$\begin{aligned} \hat{B}_1 &= \hat{I}_1^-, & \hat{B}_9 &= 2\hat{I}_1^-\hat{I}_2^z \\ \hat{B}_2 &= \hat{I}_1^z, & \hat{B}_{10} &= 2\hat{I}_1^z\hat{I}_2^z \\ \hat{B}_3 &= \hat{I}_1^+, & \hat{B}_{11} &= 2\hat{I}_1^+\hat{I}_2^z \\ \hat{B}_4 &= \hat{I}_2^-, & \hat{B}_{12} &= \hat{I}_2^+ \\ \hat{B}_5 &= 2\hat{I}_1^-\hat{I}_2^-, & \hat{B}_{13} &= 2\hat{I}_1^-\hat{I}_2^+ \\ \hat{B}_6 &= 2\hat{I}_1^z\hat{I}_2^-, & \hat{B}_{14} &= 2\hat{I}_1^z\hat{I}_2^+ \\ \hat{B}_7 &= 2\hat{I}_1^+\hat{I}_2^-, & \hat{B}_{15} &= 2\hat{I}_1^+\hat{I}_2^+ \\ \hat{B}_8 &= \hat{I}_2^z, & \hat{B}_{16} &= \hat{E}. \end{aligned} \quad [\text{A3}]$$

For $1 \leq r \leq 3$ the state described by \hat{I}_q^r has a coherence order

$$p_r = \begin{cases} -1, & r = 1 \\ 0, & r = 2 \\ 1, & r = 3 \end{cases} \quad [\text{A4}]$$

and in an external magnetic field \mathbf{B}_0 , it will precess with a frequency $\omega = -B_0\gamma_q p_r$, where γ_q is the gyromagnetic ratio of the nucleus q . Each of the states described by the \hat{B}_α will also evolve with a definite precession frequency that is characterized by its effective gyromagnetic ratio,

$$\gamma_\alpha^* = \sum_i p_{\alpha_i} \gamma_{\alpha_i}, \quad [\text{A5}]$$

where p_α and γ_α refer to the coherence order and gyromagnetic ratio of the i th operator in the product operator \hat{B}_α , respectively. The magnitude of γ_α^* determines the magnitude of dephasing (and therefore the attenuation) of the coherence described by \hat{B}_α during the application of a gradient.

Decomposition of the Spin Density Operator

First, we define the projection operator:

$$\hat{P}_{\hat{B}_\alpha} = \frac{\langle \hat{B}_\alpha |}{\langle \hat{B}_\alpha | \hat{B}_\alpha \rangle}. \quad [\text{A6}]$$

Then the projection of the operator \hat{A} onto the operator \hat{B}_α is given by

$$\hat{P}_{\hat{B}_\alpha} |\hat{A}\rangle = \frac{\langle \hat{B}_\alpha | \hat{A} \rangle}{\langle \hat{B}_\alpha | \hat{B}_\alpha \rangle}. \quad [\text{A7}]$$

It is convenient to define the decomposition function which produces from an operator, \hat{A} , a vector, \mathbf{A} , the components of which are equal to the projection of \hat{A} onto the basis operators, \hat{B}_α ,

$$D(\hat{A}) = \mathbf{A} = (\hat{P}_{\hat{B}_1} |\hat{A}\rangle, \hat{P}_{\hat{B}_2} |\hat{A}\rangle, \dots, \hat{P}_{\hat{B}_{(4^N-1)}} |\hat{A}\rangle), \quad [\text{A8}]$$

such that

$$\sum_{i=1}^{(4^N-1)} A_i \hat{B}_i = \hat{A}. \quad [\text{A9}]$$

Generating Weighted Lists of CTPs

Given a list of CTPs and their (complex) weights, it is simple to reconstruct the final spin density operator as in Eq. [8]. To generate such a list, one must consider all possible mixing caused by a Hamiltonian \hat{H} . During precession in the absence of coupling between spins, no mixing between the coherences described by the \hat{B}_α can occur, and therefore precession alone cannot cause branching in the list of CTPs. RF pulses and precession in the presence of scalar coupling or cross-relaxation can mix coherences described by the \hat{B}_α . For example, an ideal 90° RF pulse can change the coherence order of spin q by ± 1 while an ideal 180° pulse inverts the coherence order of spin q .

A general period of evolution under a Hamiltonian, \hat{H} , can be characterized by a transformation matrix that describes the evolution of each basis operator under \hat{H} . The transformation matrix can be assembled from a list of row vectors,

$$\overleftrightarrow{T} = \begin{pmatrix} D[\Re(e^{-iHt} \hat{B}_1 e^{iHt})] \\ D[\Re(e^{-iHt} \hat{B}_2 e^{iHt})] \\ \vdots \\ D[\Re(e^{-iHt} \hat{B}_{(4^N-1)} e^{iHt})] \end{pmatrix}, \quad [\text{A10}]$$

where each row vector represents the decomposition of a basis operator that has evolved under \hat{H} . The \overleftrightarrow{T} matrix contains information about all mixing of coherences caused by the evolution described by the Hamiltonian. Specifically, the element $\overleftrightarrow{T}_{ij}$ refers to the amount of mixing from \hat{B}_i to \hat{B}_j caused

by \hat{H} during time t . The transformation matrix therefore contains exactly the information necessary to generate the desired lists of weights for each CTP.

If we define the union operation on a set of vectors $\mathbf{a}^1, \mathbf{a}^2, \dots, \mathbf{a}^N$ (where each vector, \mathbf{a}^i , has components $\langle a_1^i, a_2^i, \dots, a_{n_i}^i \rangle$), as

$$\begin{aligned} \bigcup_{i=1}^N \mathbf{a}^i &= \mathbf{a}^1 \cup \mathbf{a}^2 \cup \dots \cup \mathbf{a}^N \\ &= (a_1^1, a_2^1, \dots, a_1^2, a_2^2, \dots, a_1^N, a_2^N, \dots, a_n^N), \end{aligned} \quad [\text{A11}]$$

then the list of weights for CTPs leading to the coherent state described by \hat{B}_α , after the i th Hamiltonian, will be

$$\mathbf{w}_{i+1}^{(\alpha)} = \bigcup_{j=1}^{(4^N-1)} [(T_{j\alpha})(\mathbf{w}_i^{(j)})], \quad [\text{A12}]$$

where j is an index that runs from 1 to $4^N - 1$ excluding j for which $T_{j\alpha} = 0$, and $\mathbf{w}_i^{(j)}$ is a list of weights for CTPs leading to the coherent state B_j before application of the i th H .

The associated lists of spatial frequency due to PFGs for each pathway can also be generated recursively:

$$\mathbf{k}_{i+1}^{(\alpha)} = \bigcup_{j=1}^{(4^N-1)} [\mathbf{k}_i^{(j)} + \gamma_j^* h_i]. \quad [\text{A13}]$$

Lists generated in this way have the property (implied in Eqs. [7] and [8]) that the sum of all elements in a particular $\mathbf{w}_i^{(\alpha)}$ equals the projection of the spin density at $r_z = 0$, before the application of the i th Hamiltonian, onto the operator \hat{B}_α ,

$$\sum_j (w_i^{(\alpha)})_j = \hat{P}_{\hat{B}_\alpha} \hat{\sigma}(0), \quad [\text{A14}]$$

where $(w_i^{(\alpha)})_j$ is the j th element in the list of weights of CTPs leading to coherence \hat{B}_α before the application of the i th Hamiltonian.

ACKNOWLEDGMENTS

This work was supported by NIH Grant GM-47021. D.F. acknowledges grant support (SG-00-005) from the Camille and Henry Dreyfus Foundation.

REFERENCES

1. R. H. Ernst, G. Bodenhausen, and A. Wokaun, "Principles of Nuclear Magnetic Resonance in One and Two Dimensions," Clarendon Press, Oxford (1987).
2. K. Wüthrich, "NMR of Proteins and Nucleic Acids," Wiley, New York (1986).
3. J. Cavanagh, W. J. Fairbrother, A. G. Palmer, III, and N. J. Skelton, "Protein NMR Spectroscopy," Academic Press, San Diego (1996).

4. R. P. F. Kanters, B. W. Char, and A. W. Addison, A computer-algebra application for the description of NMR experiments using the product-operator formalism, *J. Magn. Reson. A* **101**, 23 (1993).
5. P. Güntert, N. Schaefer, G. Otting, and K. Wüthrich, POMA: A complete *Mathematica* implementation of the NMR product-operator formalism, *J. Magn. Reson. A* **101**, 103 (1993).
6. S. A. Smith, T. O. Levante, B. H. Meier, and R. R. Ernst, Computer simulations in magnetic resonance. An object-oriented programming approach, *J. Magn. Reson. A* **106**, 75 (1994).
7. T. Allman, A. D. Bain, and J. R. Garbow, SIMPLTN, a program for the simulation of pulse NMR spectra, *J. Magn. Reson. A* **123**, 26 (1996).
8. A. Jerschow and N. Müller, Efficient simulation of coherence transfer pathway selection by phase cycling and pulsed field gradients in NMR, *J. Magn. Reson.* **134**, 17 (1998).
9. G. H. Meresi, M. Cuperlovic, W. E. Palke, and J. T. Gerig, Pulsed field gradients in simulations of one- and two-dimensional NMR spectra, *J. Magn. Reson.* **137**, 186 (1999).
10. J. Levine, T. Mason, and D. Broun, "Lex & Yacc," O'Reilly, Sebastopol, CA (1992).
11. M. Goldman, "Quantum Description of High-Resolution NMR in Liquids," Clarendon Press, Oxford (1988).
12. D. Fushman, S. Cahill, and D. Cowburn, The main chain dynamics of the dynamin pleckstrin homology (PH) domain in solution: Analysis of ^{15}N relaxation with monomer/dimer equilibration, *J. Mol. Biol.* **266**, 173 (1997).
13. K. Pervushin, R. Riek, G. Wider, and K. Wüthrich, Attenuated T_2 relaxation by mutual cancellation of dipole-dipole coupling and chemical shift anisotropy indicates an avenue to NMR structures of very large biological macromolecules in solution, *Proc. Natl. Acad. Sci. USA* **94**, 12366 (1997).
14. S. Braun, H.-O. Kalinowski, and S. Berger, "150 and More Basic NMR Experiments," Wiley-VCH, Weinheim (1998).
15. P. Andersson, A. Annala, and G. Otting, An α/β -HSQC- α/β experiment for spin-state selective editing of IS cross peaks, *J. Magn. Reson.* **133**, 364 (1998).